INVESTIGATION OF TWO MECHANISMS GOVERNING CLOUD CAVITATION SHEDDING: EXPERIMENTAL STUDY AND NUMERICAL HIGHLIGHT

Kilian Croci, Petar Tomov, Florent Ravelet, Amélie Danlos, Sofiane Khelladi, Jean-Christophe Robinet

INVESTIGATION OF TWO MECHANISMS GOVERNING CLOUD CAVITATION SHEDDING: EXPERIMENTAL STUDY AND NUMERICAL HIGHLIGHT

Kilian CROCI,[1] Petar TOMOV,[1] Florent RAVELET,[1] Amélie DANLOS,[2] Sofiane KHELLADI,[1] and Jean-Christophe ROBINET[1]

[1)] *DynFluid Laboratory, Arts et Métiers ParisTech, 151 Boulevard de l'Hôpital, Paris 75013, France*

[2)] *Laboratoire du Génie des Procédés pour l'Energie, l'Environnement et la Santé, Conservatoire National des Arts et Métiers, 292 rue Saint Martin, 75003 Paris, France*

Cavitation is a phenomenon of classical interest which can be observed in various applications. It consists in a transition of phase due to a pressure drop under the saturation pressure of a liquid. The unsteady behavior of this phenomenon leads to generate some issues such as erosion, noise or vibrations: as a result the comprehension of the cavity dynamics remains of crucial importance. Unsteady cavitation has been investigated in numerous studies and a mechanism of re-entrant jet has been firstly identified as responsible of the cavity shedding process. Recently, a second shedding mechanism, induced by a shock wave propagation due to the condensation of vapor structures, has been experimentally highlighted with X-ray measurements[1]*. The present paper focuses on the experimental detection, with a wavelet method, of these two shedding features on* $2D$ *image sequences recorded with a high-speed camera about a double transparent horizontal Venturi nozzle with* $18°/8°$ *convergent/divergent angles respectively. A compressible two-phase flow numerical* $3D$ *model is performed in complement in order to illustrate some phenomena hardly perceptible experimentally.*

INTRODUCTION

Partial cavity shedding phenomenon has been widely investigated in the past decades about different geometries such as hydrofoil profiles[2–7], spheres[8] or Venturi nozzles[9–12]. As a consequence, a dynamical feature has been clearly consisting of a frothy re-entrant jet reaching back the vapor cavity and eventually cutting it in two, the second "cloud" cavity being advected downstream. A correspondence between this re-entrant jet and cavity shedding occurrences has been evidenced[3]. This leads to a near-periodic cycle which can be defined with a frequency f_s. Besides Reisman et *al.*[4] observed with high-speed cameras coherent bubble collapses, due to the separated clouds convected to a high pressure region, which leads to another type of shedding phenomenon. In the recent PhD experimental works of Ganesh[1], this mechanism has been highlighted with X-Ray measurements. Such as the re-entrant jet, this shedding feature repeats itself with a frequency f_w.

The data acquired in these different studies gives valuable statistical $2D$ outcomes of the two-phase flow dynamic, such as cavity length or cloud shedding frequencies, for a large array of pressure and velocity conditions[13]. However a numerical investigation appears to be necessary to capture some phenomena which require a very high time-resolution, as the bubbly shock wave, or which are due to $3D$ effects. In this context, Schnerr et *al.*[14] focused their investigation on the collapse induced shock about a hydrofoil. In the same manner Decaix and Goncalvès[15] studied numerically the behavior of cloud cavitation developing along a Venturi type nozzle by a compressible one-fluid model. These studies point out that the major source of vorticity is due to the collapse of vapor structures which also results in the formation of hairpin vortex structures. They equally show different aspects of a periodic cycling which can take place in the case of a Venturi nozzle.

The present study proposes to investigate these two shedding processes experimentally with $2D$ image sequences recorded with a high-speed camera placed on the side of double Venturi nozzle. For a fixed Reynolds number $Re = 1.2 \times 10^5$ a small range of cavitation numbers (from $\sigma_r = 0.38$ to 0.60), corresponding to a transient cavitation regime where both shedding features are present in the flow, is explored. A wavelet method, developed by Torrence and Compo[16] and already used in cloud cavitation shedding investigations by Brandner et *al.*[8,17] is then introduced. The method is applied on image grey levels in order to extract and associate some image series to the occurrence frequencies of the two shedding mechanisms f_s and f_w. The symmetry between the two facing cavities is also discussed. Finally, a compressible $3D$ numerical model is introduced in order to highlight the bubbly shock wave mechanism, hardly perceptible in $2D$ outcomes, and to investigate the $3D$ effects on the cavities such as the "side-entrant jet" induced by aspect ratio and scale effects[10]. One can refer to the work of Tomov et *al.*[18] to have more details about the numerical models.

EXPERIMENTAL SET-UP

All experiments were carried out in the closed variable-pressure hydrodynamic loop of the DynFluid Laboratory. The circuit, fully describe in a previous work of Tomov et *al.*[12], is composed of two tanks (150 L capacity each) connected to each other with 40 mm inner diameter pipes. The test section, represented in Fig. 1, is 10 mm square

at the throat and two facing Venturi-type sections with 18°/8° convergent/divergent angles respectively induce vapor/liquid mixture cavities. All positions in the test section are expressed as non-dimensional values $X^\star$ originating at the center of the test section.

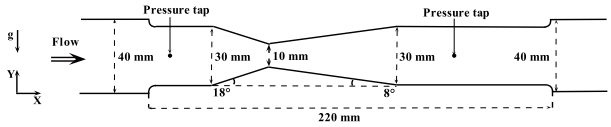

FIG. 1. VENTURI NOZZLE GEOMETRY AT SCALE[12].

The operating discharge velocities in the pipes V_{in} and at the throat V_r are estimated regarding the flow-rate measurements and are kept constant in all the study; respectively at 4 and 12 m.s^{-1}. In the mean time the pressure P, measured upstream of the throat at $X^\star = -6$, is varied in the present set from 94 to 110 kPa. The reference pressure at the Venturi throat P_r is estimated with a classical Bernoulli theorem (assuming there is no pressure loss between the upstream and the throat part) as follow $P_r = P + \frac{1}{2}\rho(V_{in}^2 - V_r^2)$. All the characteristic non-dimensional numbers associated to the present study, which are based on the reference values at the throat P_r, V_r, and H, are developed in Tab. I. The Strouhal number, for which the definition remains intricate in spite of the proposal of its unification made by Dular[19], is defined in the present study with the Venturi throat height H in order to only observe the evolution of the shedding frequencies independently of the cavity closure length.

TABLE I. NON-DIMENSIONAL NUMBERS.

	FORMULATION
$X^\star$	$\frac{x}{H}$
Re	$\frac{HV_r}{\nu}$
σ_r	$\frac{(P_r - P_v)}{\frac{1}{2}\rho V_r^2}$
St	$\frac{fH}{V_r}$

High-speed photography was used to investigated the cloud cavitation shedding mechanisms. The camera, placed on the side of the Venturi nozzle, acquired image sequences with a resolution of 1280 × 512 pixels within 1000 frames per second during 3 seconds. One can refer to the study of Tomov et *al.*[12] for further informations about the experimental set-up characteristics and the uncertainties of measurements.

EXPERIMENTAL OUTCOMES ANALYSIS

In the present paper a transient cavitation regime (also called "transitory regime"[1]) where two shedding mechanisms coexist is investigated. This particular regime, studied for a fixed Reynolds number $Re = 1.2 \times 10^5$, occurs in the present study for an array of cavitation numbers between 0.38 and 0.60. The following subsections present the different post-processing techniques used to extract the shedding cavity characteristics in order to investigate the different mechanisms in addition to the cavities' symmetry.

Grey Level Detection

Classically the cavity closure length, which correspond to the place where most of the shedding processes take place, is detected with the maximum of standard deviation on a sequence of images[11]. In the present study the region of interest is divided in two in order to investigate the symmetry of the different cavities. After image normalization, consisting in subtracting all instantaneous images by a reference image without cavitation, the grey levels are calculated in all the image series and the maximum of standard deviation is detected as visible in Fig. 2. Averaging in all the image sequence, the two facing cavities appears to be symmetrical and for the cavitation number reported in Fig. 2, the cavity closure length measured is almost the same for both sided cavities ($L^\star \simeq 4.05$).

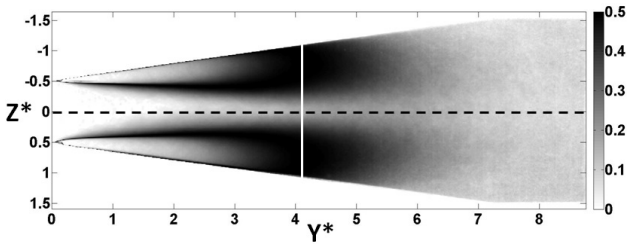

FIG. 2. STANDARD DEVIATION FOR AN IMAGE SEQUENCE TAKEN AT $\sigma_r = 0.46$. THE WHITE FULL LINE REPRESENT THE CAVITY CLOSURE LENGTH CORRESPONDING TO A MAXIMUM OF STANDARD DEVIATION.

After this first step, a frequency analysis is made on the grey level signals extracted from the vertical line associated to the cavity closure (white full line in Fig. 2) to capture the shedding frequencies supposedly associated to both shedding phenomena.

Wavelet Frequency Analysis

Wavelet analysis is usually used, mainly in geophysics studies, in order to decompose time signals into time-frequency space allowing to determine dominant modes of variability through time and, as a result, to associate dynamic features to their frequencies of occurrence. This method is particularly adapted to detect near-periodic events such as cloud cavitation shedding phenomena that can occur simultaneously.

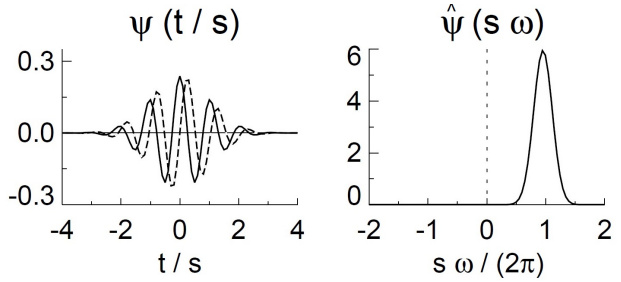

FIG. 3. MORLET WAVELET BASE REPRESENTATION IN TIME DOMAIN (LEFT) AND IN CORRESPONDING FREQUENCY DOMAIN AFTER WAVELET TRANSFORM (RIGHT). THE LEFT PLOT GIVE THE REAL PART (SOLID) AND THE IMAGINARY PART (DASHED). FROM TORRENCE AND COMPO[16].

In the present study a continuous wavelet transform based on the work of Torrence and Compo[16] is applied on grey level signals at the cavity closure line. A non-orthogonal complex wavelet function, relevant for time series analysis, is implemented with a Morlet base (Fig. 3). This particular wavelet base, representing a plane wave modulated by a Gaussian, is particularly adapted and usually used with image analysis to extract frequencies of occurrence[8]. Consequently, the method give the wavelet transform $|W_n|$ all along image series in time-frequency space allowing to associate a particular sequence of images (representing for instance a shedding process) to an array of frequency. By integration on the time series, a Power Spectral Density (PSD) $|Wn|^2$ can be calculated and a frequency of occurrence can be estimated.

An example of application is given in Fig. 4 in a particular case ($\sigma_r = 0.38$) which will permit to illustrate the two shedding mechanisms in the following. Firstly one can notice similarities between the two wavelet transforms, confirming the symmetry between top and bottom cavities. Secondly the PSD associated to both facing cavities presents two similar frequency peaks which might correspond to the two shedding frequencies pursued.

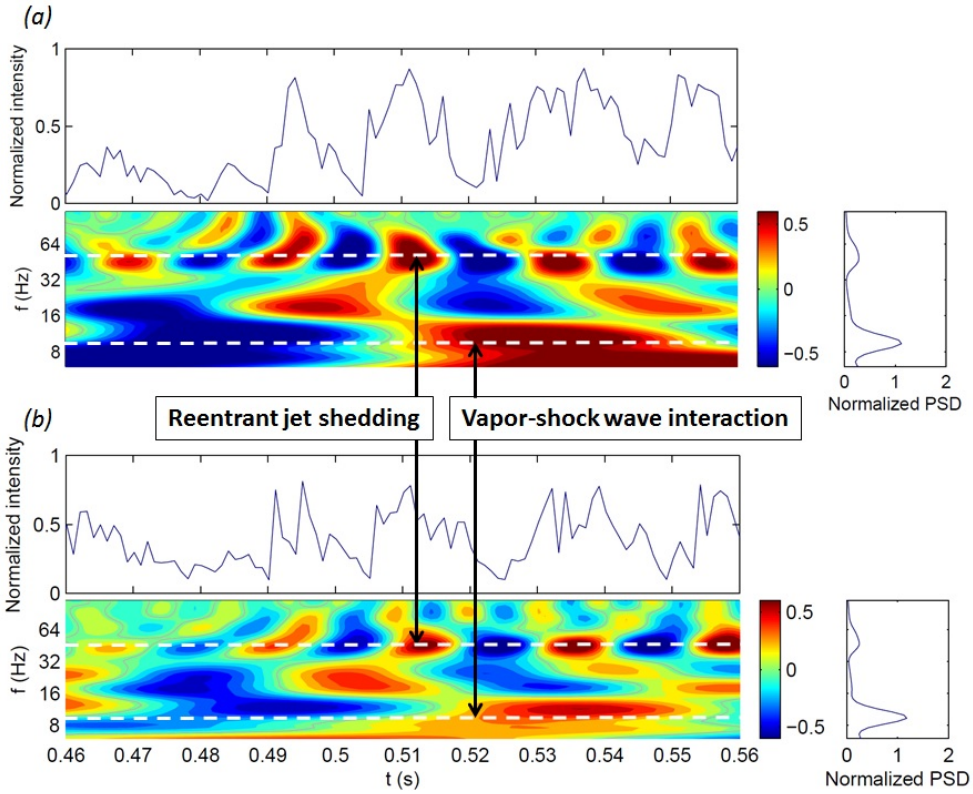

FIG. 4. TIME SERIES OF GREY LEVEL TAKEN AT CAVITY CLOSURES BETWEEN 460 AND 560 MS FOR $\sigma_r = 0.38$, CORRESPONDING WAVELET TRANSFORM AND POWER SPECTRAL DENSITY (PSD) FOR (A) TOP AND (B) BOTTOM CAVITIES. IDENTIFICATION OF FREQUENCIES f_s AND f_w.

Transient Cavitation Regime

As a result, both evolutions of cavity closure lengths $L^\star$ and shedding frequencies f_s and f_w are obtained experimentally with image analysis as a function of the cavitation number in the transient cavitation regime (Fig. 5).

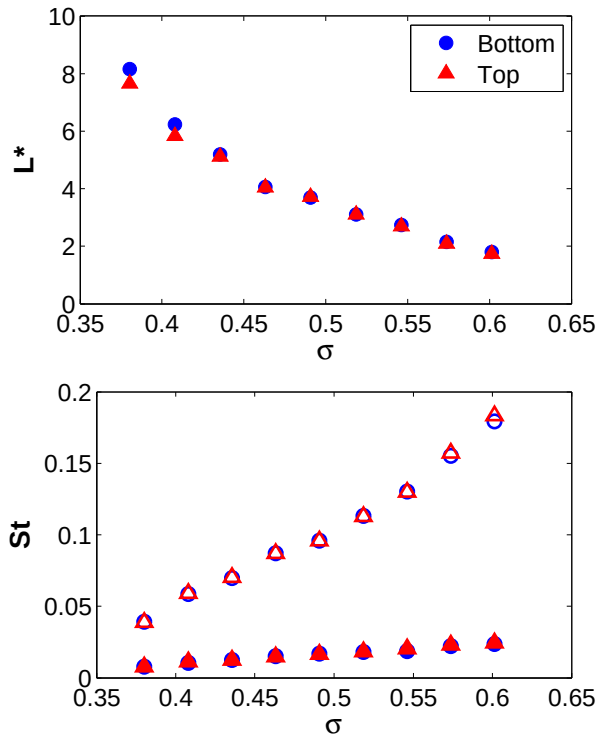

FIG. 5. (A) NON-DIMENSIONAL CAVITY LENGTH CLOSURE AND (B) BUBBLY SHOCK WAVE (CLOSED SYMBOLS) AND RE-ENTRANT JET (OPEN SYMBOLS) SHEDDING FREQUENCIES EVOLUTIONS ACCORDING TO THE CAVITATION NUMBER. COMPARISON BETWEEN TOP (TRIANGLES) AND BOTTOM (CIRCLES) CAVITIES.

The evolution of the cavity closure length is found to be in good agreement with the literature[9,11,13] for both top and bottom cavities which have almost the same size for a given pressure. On the other hand the two measured frequency peaks appears to increase differently with the cavitation number. The lower shedding frequency (about 10 Hz), which might correspond to f_w according to the wavelet transform outcomes, is increasing slowly with the cavitation number whereas the associated re-entrant jet shedding frequency f_s increases faster, the frequency quadrupling from 50 to 200 Hz between $\sigma_r = 0.38$ and $\sigma_r = 0.60$. Therefore the re-entrant jet mechanism seems to be highly influenced by the cavity size, the shedding feature occurring with more difficulty for long cavities. These results are coherent with the outcomes obtained by Keil et *al.*[13] who detected two periodic processes progressing as a function of the cavitation number in the same way than in the present study. These two shedding frequencies have also been reported by Leroux et *al.*[7] who observed, for an hydrofoil, a frequency peak about 18 Hz corresponding to a re-entrant jet shedding and a lower frequency (about 3.5 Hz) that they associated to a shock wave phenomenon induced by the main cloud collapse. One can notice equally that the symmetry between top and bottom cavities appears to begin to break for the lowest cavitation numbers with the cavity lengths. The evolution of the shedding frequencies, with the diminution of the re-entrant jet shedding frequency for low cavitation number, might indicate a transition to another cavitation regime: the "periodic" cavitation regime (where only the bubbly shock wave occur) reported by Ganesh[1].
This transition of shedding mechanism has been characterized by several authors[6,15] by a cavity length bifurcation around the value $\sigma/2\alpha \simeq 4$ where α represents the attack angle of an hydrofoil and the divergent angle in a simple Venturi-type geometry. In the present study $\alpha = 8°$ and σ can be defined with the inlet pressure P (assuming the pressure loss between the upstream and the cavity closure is negligible) and the flow velocity V_r which is supposed to be reached at the cavity closure. Thus the lowest pressure investigated, for which the re-entrant jet frequency is very low, corresponds to $\sigma/2\alpha \simeq 4.57$ which is coherent with the cavity length bifurcation classical value.

NUMERICAL SIMULATIONS

Numerical simulations ($\sigma_r = 0.26$) are used in complement to highlight the bubbly shock wave mechanism, hardly perceptible in the previous experimental image series, and to capture a feature due to $3D$ effects: the side-entrant jet. The numerical model consists in a compressible Navier-Stokes equations coupled with the Homogeneous Equilibrium Mixture model (HEM) which are solved with a Finite Volume solver based on Moving Least Squares (MLS) approximations. The computational domain, based on the experimental geometry, is meshed with 3.1×10^5 tetrahedral cells.
Due to the compressibility of the two phases, spurious pressure waves might be generated from the upstream and downstream boundaries and then trapped in the computational domain. In order to overcome to this problem, the same non-reflecting boundary conditions as the ones used by Schnerr et *al.*[14] are computed. Velocity V_{in} and temperature T_∞ are imposed in the inlet boundary in addition to a static pressure P_o at the outlet boundary. Table II summarizes these boundary conditions.
In the present study, a really small time step is necessary in order to capture the different shedding mechanisms. To date coherent frequencies of shedding cannot be found properly with simulations and compared with experimental data, therefore the numerical investigation will only be focused on the description of the shedding features.

TABLE II. BOUNDARY CONDITIONS IN COMPUTATION.

V_{in}	P_o	P	T_∞	Re	σ_r
$(m.s^{-1})$	(kPa)	(kPa)	(K)		
4	50	85	300	1.2×10^5	0.26

The numerical models and the meshing is further detailed in the work Tomov et *al.*[18].

CLOUD CAVITATION SHEDDING MECHANISMS

In the present section, several shedding mechanisms are discussed. The choice is made to focus the experimental study, which is based on the wavelet analysis visible in Fig. 4, only on the extreme cavitation number $\sigma_r = 0.38$. The vapor structures are in that case of important size and consequently might be easier to observe. As reported in Tab. III, one can notice that the wavelet PSD peak ratio $R = |W_n(f_w)|^2/|W_n(f_s)|^2$ is important, meaning that the bubbly shock wave phenomenon is particularly pronounced comparing to the re-entrant jet and, as a result, might be visible in images in spite of the quickness of the wave.

TABLE III. EXPERIMENTAL RESULTS FOR $\sigma_r = 0.38$.

	Bottom Cavity	Top Cavity	Uncertainty
f_s (Hz)	47.2	48.2	±4%
f_w (Hz)	9.5	9.5	±4%
$L^\star$	8.2	7.7	±2%
R	4.8	3.9	±10%

Re-Entrant Jet

As previously explained, the re-entrant jet is a well-known shedding mechanism characterized in several studies[2,3,6]. This cloud shedding cycle is illustrated in Fig. 6 with experimental side views.
The re-entrant jet occurs at the rear of the cavity due to the expansion of its closure region; the combination with the wall induces a stagnation point. The conservation of momentum at this point makes the fluid to go under the cavity: a re-entrant jet is created. For small cavities, the jet thickness is very small comparing to the frothy cavity thickness and an adverse pressure peak tends to stabilize the cavity closure. It results in a closed cavity where the re-entrant jet generates an apparently coherent and robust in time vapor/liquid mixture. For big cavities, as presented in Fig. 6, the adverse pressure gradient at cavity closure is small enough in order that the frothy re-entrant jet, generated after the cavity growing ($T = 498$ ms), progresses in the vapor phase ($T = 500$ to 510 ms) and finally reaches its top surface interface. As a result the vapor phase is cut in two parts ($T = 512$ ms), the downstream partial cavity being next advected by the flow. One can notice equally the creation of a hairpin-like vortex, highlighting the interaction between the top and bottom cavities.

The re-entrant jet shedding cycle presented in Fig. 6 (and more precisely the last sequence image taken at $T = 512$ ms), is identified in Fig. 4 corresponding to the peak of wavelet transform associated to a frequency of occurrence f_s. As a result, the cloud cavitation shedding due to the re-entrant jet can be associated with the higher frequency identified experimentally with the wavelet method f_s.

Bubbly Shock Wave

As described in the experimental PhD work of Ganesh[1], the condensation shock wave might occur at the cavity closure when the thickness of the re-entrant jet tends to be equal to the cavity thickness (contrary to the re-entrant jet shedding mechanism for which the jet thickness is small comparing to the cavity thickness) which does not enable the flow to attain a kinematic equilibrium. Indeed, this equality would require that the flow streamline at the cavity interface turn sharply of 180° at the rear, implying no kinematic equilibrium in the flow. Instead of this unstable phenomena, a propagating discontinuity is observed[1] which might be due to the sudden stop of the cavity growth generating an overpressure region downstream of the cavity. This overpressure might then interact with a "cloud" vapor structure previously detached by one of the shedding mechanisms, implying an abrupt condensation of the structure. As a consequence, the bubbly structure imploded and a coherent condensation (or bubbly) shock wave is eventually created (as observable in the numerical snapshots presented in Fig. 7).

In particular flow conditions, where the cavity vapor/liquid mixture is of important size and thus not very dense, the local speed of sound can become very small and a high local Mach numbers can be reached. This flow change results in a slower propagation of any potential disturbances, such as the condensation shock wave, in the vapor structures than in liquid modifying the characteristic time scales in the flow. It leads to the presence of a propagating condensation shock wave which might interact with the cavity closure region. This shock wave could then be spread to the rest of the cavity inducing some reflections and vapor condensations resulting to a possible complex massive cloud cavitation shedding.

In the present study, the experimental data available

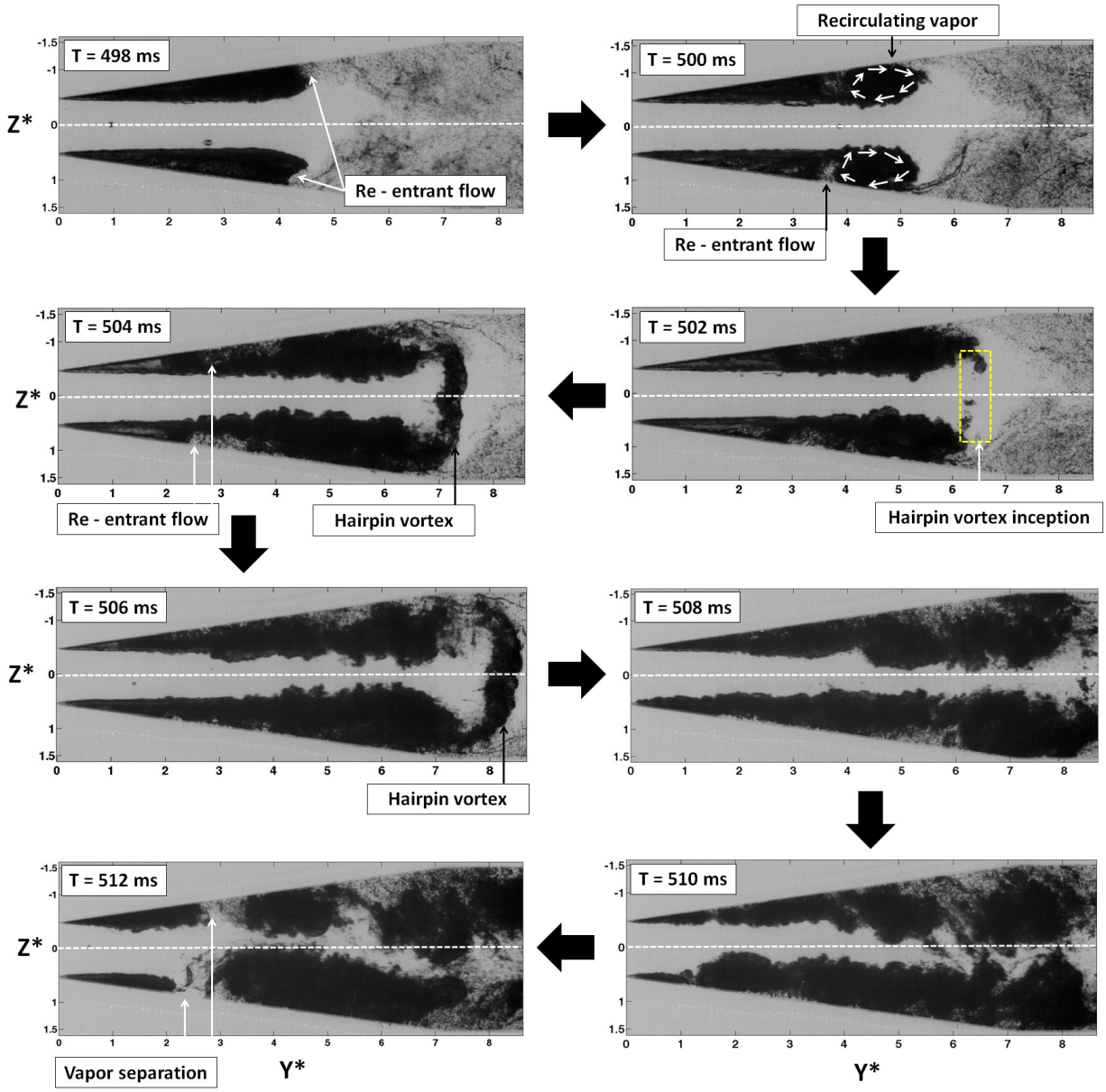

FIG. 6. EXPERIMENTAL IMAGE SEQUENCE TAKEN AT CAVITY CLOSURE BETWEEN 498 AND 510 MS FOR $\sigma_r = 0.38$ AND CORRESPONDING TO THE FIRST WAVELET TRANSFORM PEAK PRESENTED IN FIG. 4. DARK REGIONS ARE INDICATIVE OF VAPOR AND LIGHTER REGIONS OF LIQUID PHASE.

show that an intricate shedding process occurs periodically with a frequency f_w but do not permit to access to a clear description of the condensation shock wave phenomenon. As a result a numerical investigation, in connexion with the pertinent experimental outcomes on the mechanism available in the literature[1], appears to be necessary in order to explore the shedding feature.

Therefore, Fig. 7 gives a preview of the condensation of a vapor cloud described in the previous paragraphs. One can notice the diminution of the vapor structure downstream, which can be associated to a local velocity divergence[12], leading to an implosion of the bubbly structure. The shock wave generated by this implosion is then propagated in the flow ($T = 41.3$ ms). A pressure value of 673 kPa is measured in the simulation at the location of this implosion which is coherent with the instanteous maximum pressure of 105 bar numerically obtained by Schnerr et *al.*[14]. The interaction of this shock wave with the two facing cavities is presented numerically in Fig. 8 and experimentally. in Fig. 9.

The interaction between a bubbly shock wave (also called condensation shock wave) and the vapor structures is first captured experimentally in the image series at $T = 520$ ms (Fig. 9) and is identified in the wavelet transform (Fig. 4) as the beginning of a shed-

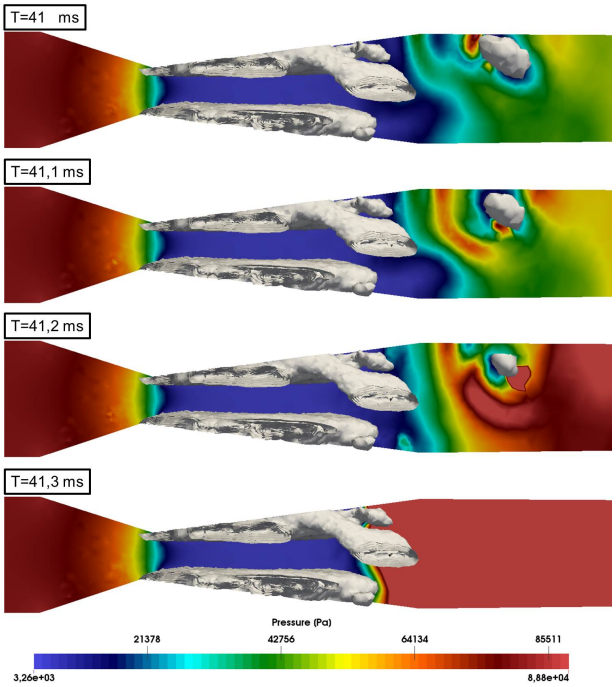

FIG. 7. NUMERICAL SNAPSHOTS OF THE PRESSURE DISTRIBUTION AND THE VAPOR STRUCTURES FOR $\sigma_r = 0.26$ WITH A TIME STEP OF 0.1 MS. THE MAXIMUM PRESSURE IS SATURATED AT 8.88×10^4 PA TO VISUALIZE THE PROCESS OF CONDENSATION.

ding process characterized by a frequency f_w. This interaction, extremely difficult to capture experimentally due to the quickness of the phenomenon, presents the existence of characteristic vertical sharp edges which have equally been observed experimentally by Ganesh[1].

Numerically, the resulting shedding process is presented in Fig. 8 between 40 ms and 50 ms. At $T = 40$ ms, a cloud shedding due to a re-entrant jet just finishes and a vapor structure is advected downstream. After 250 μs the cloud structure has imploded (Fig. 8) and the resulting condensation shock is propagating in all directions in the flow. The following images in the sequence, taken with a time step of 1 ms, show the interaction of the shock wave with top and bottom vapor cavities. As a result a contraction of both cavities, which might be due to this interaction, is observed between the two snapshots taken at $T = 41.25$ and $T = 43$ ms. The sizes of both top an bottom cavities appears to be synchronized and symmetrical in the horizontal direction. The shock wave is then propagating in the frothy cavities with a very small velocity due to the different gas fractions encountered. The propagation velocity is estimated in the present numerical results about 5 $m.s^{-1}$ (for a time period of 3.5 ms the shock wave moves forward 17.6 mm) which is coherent with the outcomes of Ganesh[1]. In the rest of the sequence, several little vapor shedding processes and cavity/condensation shock wave interactions are observed until that a major shedding occurs at $T = 50$ ms. These observations concur with the experimental image sequences registered where this shedding feature appears to endure several interactions. Finally between the beginning ($T = 41.25$ ms), where the shock wave has not had affected the vapor cavities, and the end ($T = 50$ ms) of the shedding cycle the cavity lengths of both sides of the Venturi nozzle $L^\star$ decreased from 6 to 2. This decrease confirms the importance of the condensation shock wave as an unsteady cloud shedding process.

To resume, the condensation shock wave shedding mechanism has been identified numerically and the observations obtained are in good agreement with the experimental analysis of Ganesh[1]. Furthermore one can notice that the mechanism leading to the apparition of a condensation shock wave, which combines a cloud of vapor (previously shed by a re-entrant jet) and a cavity which reaches its maximum size of stability, induces that the frequency of occurrence of this event might be lower than the re-entrant jet shedding frequency. This assumption is consistent with the experimental results found in the previous sections.

3D Feature: the Side-Entrant Jet

The numerical simulations are equally used in order to capture $3D$ effects, non-accessible with $2D$ experimental measurements. As a result, a modified re-entrant jet process called "side-entrant jet" is observed numerically and is illustrated in Fig. 10.
This $3D$ phenomenon has been noticed experimentally with Venturi geometries in the works of Dular et *al.*[10] and numerically with hydrofoils by Schnerr et *al.*[14]. According to these studies this feature might be due to scale effects and aspect ratios. The side-entrant jet can occur under certain conditions of containment (with small and wide Venturi throat sections) for which the re-entrant jet is deviated randomly on both sides. In the present study, one can notice a transversal flow velocity at the Venturi throat (Fig. 10) evolving from the side walls to the middle section of the nozzle. This phenomenon then leads, as the same manner as the classical re-entrant jet, to a vapor cloud shedding.

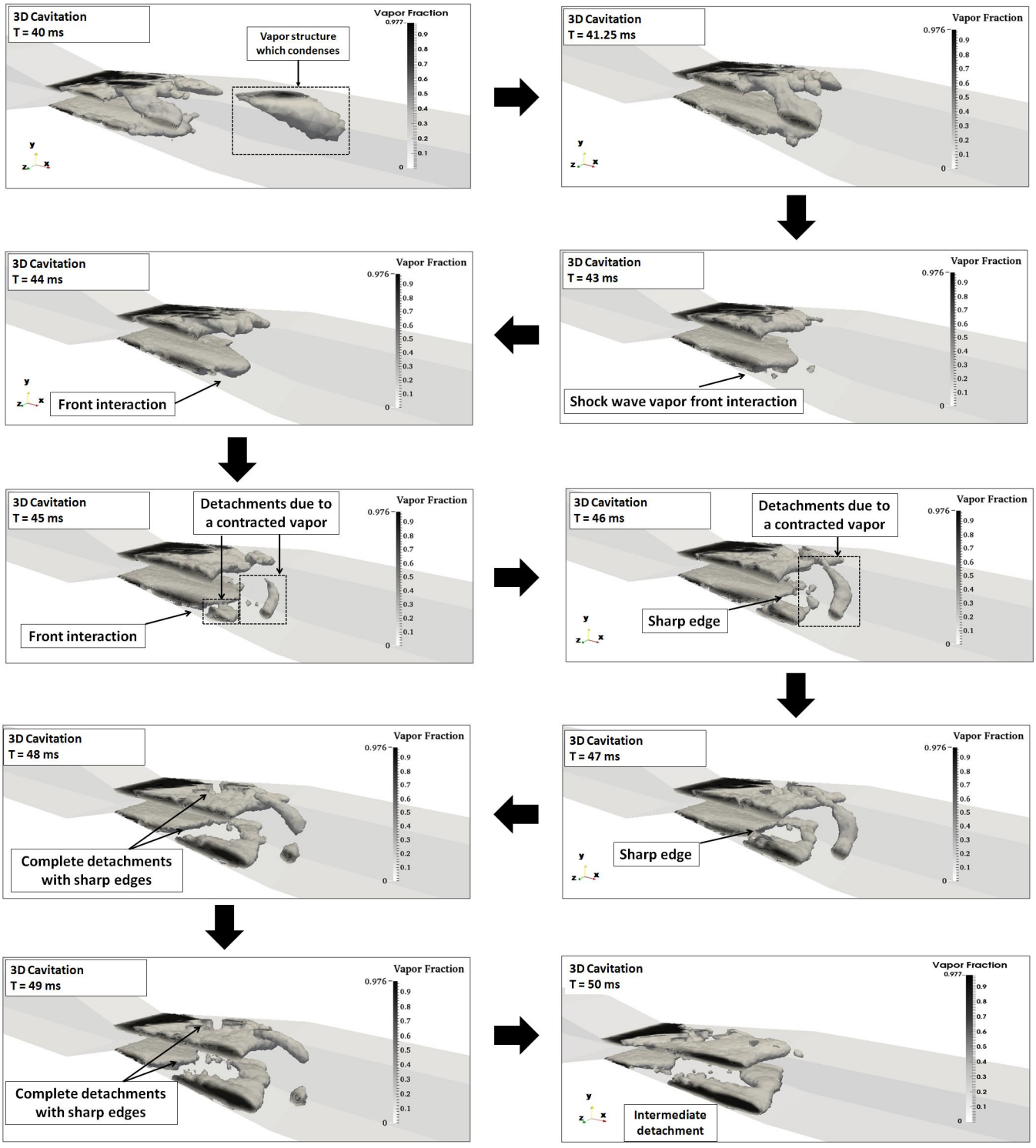

FIG. 8. NUMERICAL SNAPSHOTS OF THE PRESSURE DISTRIBUTION FOR $\sigma_r = 0.26$ WITH A TIME STEP OF 0.1 MS. HIGHLIGHT ON THE VAPOR STRUCTURE CONDENSATION.

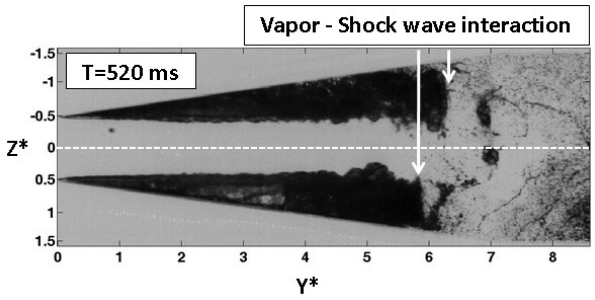

FIG. 9. NORMALIZED EXPERIMENTAL SNAPSHOT TAKEN AT $T = 520$ MS FOLLOWING THE SEQUENCE EXPOSED IN FIG. 6 SHOWING THE INTERACTION BETWEEN THE VAPOR STRUCTURES AND A CONDENSATION SHOCK WAVE.

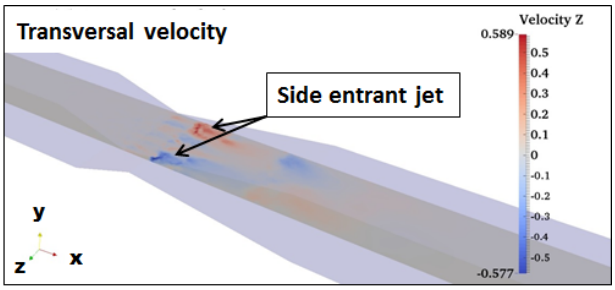

FIG. 10. NUMERICAL SNAPSHOTS OF THE TRANSVERSAL VELOCITY AT THE VENTURI THROAT FOR $\sigma_r = 0.26$ HIGHLIGHTING THE SIDE-ENTRANT JET PHENOMENON.

CONCLUSIONS

In the present paper, the transient cavitation regime has been investigated experimentally on $2D$ image sequences in addition to $3D$ numerical simulations which illustrate the shedding mechanisms hardly perceptible on image series. The following summarizes the important conclusions.

(1): Two different mechanisms have been clearly identified as responsible of cavitation cloud shedding in the transient cavitation regime, namely the **re-entrant jet** and the **condensation shock wave**.

(2): The condensation shock wave shedding mechanism has been described with numerical simulations and the resulting observations are found to be in good agreement with the conclusions made in the experimental investigation of Ganesh[1]. Consequently the shock wave appears to result to the condensation (and the implosion) of a vapor structure which has been previously shed from the cavity downstream. This condensation feature might be induced by a sudden stop of the cavity growth (due to kinematic equilibrium conservation) which generate an overpressure region downstream of the cavity. The cloud shedding resulting appears in experimental photography to be too complex for a clear description of the physic dynamic because of the multiple little vapor detachments in addition to the shock/cavity interactions.

(3): The classic re-entrant jet mechanism has been fully described with experimental data and a side-entrant jet phenomenon, which implies the deviation of the re-entrant jet due to scale effects, has been identified as a pure $3D$ mechanism only visible on numerical simulations.

(4): Two dynamical features, namely the condensation shock wave and the combination of re-entrant and side-entrant jets have been statistically associated, with a wavelet method, to two shedding frequencies f_w and f_s, respectively. The condensation shock wave frequency f_w (about 10 Hz) is found to be lower than f_s (from 50 to 200 Hz). This result is coherent with the experimental observations available in scientific literature and with the description of the phenomenon.

(5): In the transient cavitation regime, the cavity length appears to evolute classically as a function of the pressure and a certain symmetry is observed between top and bottom cavities. This symmetry is also obtained regarding the evolution of the shedding frequencies.

FUTURE DEVELOPMENTS

The study of shock waves induced by cloud collapses has become a main field of interest in the cavitation investigations as evidenced by the recent works of Ganesh[1], Tomov et *al.*[18], Dular and Petkovšek[20] or Gnanaskandan and Mahesh[21,22]. The following of the present study would consist in the development of the numerical method and its validation with adapted experimental investigations focusing mainly on the condensation shock wave shedding mechanism.

REFERENCES

[1]Ganesh, H., 2015. "Bubbly shock propagation as a cause of sheet to cloud transition of partial cavitation and stationary cavitation bubbles forming on a delta wing vortex". PhD thesis, University of Michigan.

[2]Le, Q., Franc, J.-P., and Michel, J.-M., 1993. "Partial cavities: global behavior and mean pressure distribution". *J. Fluids Eng.,* ***115***, pp. 243–248.

[3]Pham, T., Larrarte, F., and Fruman, D., 1999. "Investigation of unsteady sheet cavitation and cloud cavitation mechanisms". *J. Fluids Eng.,* ***121***, pp. 289–296.

[4]Reisman, G. E., Wang, Y.-C., and Brennen, C. E., 1998. "Observations of shock waves in cloud cavitation". *J. Fluid Mech.,* ***355***, pp. 255–283.

[5]Kjeldsen, M., Arndt, R. E. A., and Effertz, M., 2000. "Spectral Characteristics of Sheet/Cloud Cavitation". *J. Fluids Eng.,* ***122***, pp. 481–487.

[6]Callenaere, M., Franc, J. P., Michel, J., and Riondet, M., 2001. "The cavitation instability induced by the development of a re-entrant jet". *J. Fluid Mech.,* ***444***, pp. 223–256.

[7]Leroux, J.-B., Coutier-Delgosha, O., and Astolfi, J. A., 2005. "A joint experimental and numerical study of mechanisms associated to instability of partial cavitation on two-dimensional hydrofoil.". *Phys. Fluids,* ***17***, p. 052101.

[8]Brandner, P., Walker, G. J., Niekamp, P. N., and Anderson, B., 2010. "An experimental investigation of cloud cavitation about a sphere". *J. Fluid Mech.,* ***656***, pp. 147–176.

[9]Stutz, B., and Reboud, J.-L., 2000. "Measurements within unsteady cavitation". *Exp. In Fluids,* ***29***, pp. 545–552.

[10]Dular, M., Khlifa, I., Fuzier, S., Adama Maiga, M., and Coutier-Delgosha, O., 2012. "Scale effect on unsteady cloud cavitation". *Exp. In Fluids,* ***53***, pp. 1233–1250.

[11]Danlos, A., Méhal, J. E., Ravelet, F., Coutier-Delgosha, O., and Bakir, F., 2014. "Study of the cavitating instability on a grooved venturi profile". *Int. J. Heat and Fluid Flow,* ***136***, p. 101302.

[12]Tomov, P., Khelladi, S., Ravelet, F., Sarraf, C., Bakir, F., and Vertenoeuil, P., 2016. "Experimental study of aerated cavitation in a horizontal venturi nozzle". *Exp. Thermal and Fluid Science,* ***70***, pp. 85–95.

[13]Keil, T., Pelz, P. F., and Buttender, J., 2012. "On the transition from sheet to cloud cavitation". In 8th Int. Symp. on Cavitation.

[14]Schnerr, G. H., Sezal, I. H., and Schmidt, S. J., 2008. "Numerical investigation of three-dimensional cloud cavitation with special emphasis on collapse induced shock dynamics". *Phys. Fluids,* ***20***.

[15]Decaix, J., and Goncalvès, E., 2013. "Investigation of three-dimensional effects on a cavitating venturi flow". *Int. J. Heat and Fluid Flow,* ***44***, pp. 576–595.

[16]Torrence, C., and Compo, G. P., 1999. "A practical guide to wavelet analysis". *Bull. Amer. Meteor. Soc,* ***79***.

[17]Brandner, P., Pierce, B. W., and de Graaf, K. L., 2015. "Cavitation about a jet in crossflow". *J. Fluid Mech.,* ***768***, pp. 141–174.

[18]Tomov, P., Croci, K., Khelladi, S., Ravelet, F., Danlos, A., Bakir, F., and Sarraf, C., 2016. Experimental and numerical investigation of two physical mechanisms influencing the cloud cavitation shedding dynamics. "See also URL `https://hal.archives-ouvertes.fr/hal-01284006v1`", March.

[19]Dular, M., and Bachert, R., 2009. "The issue of strouhal number definition in cavitating flow". *J. of Mech. Eng.,* ***55***, pp. 666–674.

[20]Dular, M., and Petkovšek, M., 2015. "On the mechanisms of cavitation erosion coupling high speed videos to damage patterns". *Exp. Thermal and Fluid Science,* ***68***, pp. 359–370.

[21]Gnanaskandan, A., and Mahesh, K., 2016. "Numerical investigation of near-wake characteristics of cavitating flow over a circular cylinder". *J. Fluid Mech.,* ***790***, pp. 453–491.

[22]Gnanaskandan, A., and Mahesh, K., 2016. "Large eddy simulation of the transition from sheet to cloud cavitation over a wedge". *Int. J. Multiphase Flow,* ***83***, pp. 86–102.